Vol.24, October.2015 ISSN 2354-7065

Journal of Ocean, Mechanical and Aerospace

-Science and Engineering-

ISOMAse

International Society of Ocean, Mechanical and Aerospace, Scientists and Engineers

Journal of Ocean, Mechanical and Aerospace
-Science and Engineering-
Vol.24: October 30, 2015

Contents

ISOMAse

International Society of Ocean, Mechanical and Aerospace
-Scientists and Engineers-

Journal of Ocean, Mechanical and Aerospace
-Science and Engineering-
Vol.24: October 30, 2015

About JOMAse

The **Journal of Ocean, Mechanical and Aerospace -science and engineering- (JOMAse, ISSN: 2354-7065)** is an online professional journal which is published by the International Society of Ocean, Mechanical and Aerospace -scientists and engineers- (ISOMAse), Insya Allah, twelve volumes in a year. The mission of the JOMAse is to foster free and extremely rapid scientific communication across the world wide community. The JOMAse is an original and peer review article that advance the understanding of both science and engineering and its application to the solution of challenges and complex problems in naval architecture, offshore and subsea, machines and control system, aeronautics, satellite and aerospace. The JOMAse is particularly concerned with the demonstration of applied science and innovative engineering solutions to solve specific industrial problems. Original contributions providing insight into the use of computational fluid dynamic, heat transfer, thermodynamics, experimental and analytical, application of finite element, structural and impact mechanics, stress and strain localization and globalization, metal forming, behaviour and application of advanced materials in ocean and aerospace engineering, robotics and control, tribology, materials processing and corrosion generally from the core of the journal contents are encouraged. Articles preferably should focus on the following aspects: new methods or theory or philosophy innovative practices, critical survey or analysis of a subject or topic, new or latest research findings and critical review or evaluation of new discoveries. The authors are required to confirm that their paper has not been submitted to any other journal in English or any other language.

ISOMAse

International Society of Ocean, Mechanical and Aerospace
-Scientists and Engineers-

Journal of Ocean, Mechanical and Aerospace
-Science and Engineering-
Vol.24: October 30, 2015

Scope of JOMAse

The JOMAse welcomes manuscript submissions from academicians, scholars, and practitioners for possible publication from all over the world that meets the general criteria of significance and educational excellence. The scope of the journal is as follows:

- Environment and Safety
- Renewable Energy
- Naval Architecture and Offshore Engineering
- Computational and Experimental Mechanics
- Hydrodynamic and Aerodynamics
- Noise and Vibration
- Aeronautics and Satellite
- Engineering Materials and Corrosion
- Fluids Mechanics Engineering
- Stress and Structural Modeling
- Manufacturing and Industrial Engineering
- Robotics and Control
- Heat Transfer and Thermal
- Power Plant Engineering
- Risk and Reliability
- Case studies and Critical reviews

The International Society of Ocean, Mechanical and Aerospace –science and engineering is inviting you to submit your manuscript(s) to admin@isomase.org for publication. Our objective is to inform authors of the decision on their manuscript(s) within 2 weeks of submission. Following acceptance, a paper will normally be published in the next online issue.

ISOMAse

International Society of Ocean, Mechanical and Aerospace
-Scientists and Engineers-

Journal of Ocean, Mechanical and Aerospace
-Science and Engineering-
Vol.24: October 30, 2015

Editors

ISOMAse

International Society of Ocean, Mechanical and Aerospace
-Scientists and Engineers-

Journal of Ocean, Mechanical and Aerospace
-Science and Engineering-, Vol.24

October 30, 2015

Estimation of Capacity and Center of Weight of Traditional Ship, Bagan Siapiapi

Yohanes,[a,*] Muftil Badri,[a] and Pindo Evans Manuel Damanik,[a]

[a)]*Mechanical Engineering, Universitas Riau, Indonesia*

*Corresponding author: yohanes_tmesin@yahoo.com

Paper History

Received: 2-October-2015
Received in revised form: 27-October-2015
Accepted: 29-October-2015

ABSTRACT

On traditional manufactures fishing boats in Indonesia, especially in the shipyard at Bagan Siapiapi, on Riau province usually made by rely on the ability of inherited tradition and hereditary not based on function and their designation. Example that way still used when determine capacity and center of gravity. This research aims to study capacity and center gravity of ship nets at Bagan Siapiapi using computer simulations. On this method some of data about capacity, center of gravity, drawing design and construction of ships would to be studied systematic and accurate base on practical condition. That case would be studied and validate on the one shipyard industry at Bagan Siapiapi. Some result from this study are (1) Capacity of ship nets 7093 kg and the weight is 13401.04 kg on the full condition. (2) Center weight of ship nets at X = 0.7mm; Y = 888.5mm; and Z = -162.5 mm. (3) Stability of ship nets on the without load has a smaller tilt angle compare than the full load condition.

KEY WORDS: *Ship nets, capacity, center of weight*

1.0 INTRODUCTION

Indonesia is maritime country which two-thirds territory is ocean. Amount area of the sea shown that Indonesian is state which potential resources of fish. This resources can bring benefits in utilization if would be supported in good condition on facilitate and infrastructure. If we want increasing in the utilization of ocean that will be required attempt and efforts to increase amount of fishing ship. Fishing ships are vessels that be used in fishing business which involves utilize or caught of or collecting water resources, processing in aquaculture or in anything else like research, training and inspection of ocean resources [1].

Some of fishing ships consist of many different size and shape. The small ones from wooden driving by oar or sail and the big vessel made by steel. Capacity of the ship that would be built on the shipyard have different characteristic from one shipyard to another. It can depend on fisheries business, usually restricted by capital. Generally there are two ways of making fishing ships in Indonesia :

1) traditional,
2) modern.

On traditional manufactures fishing boats in Indonesia, especially in the shipyard at Bagan Siapiapi, on Riau province usually made by rely on the ability of inherited tradition and hereditary didn't based on function and their designation. Instance of capacity and center of weight those are defined using traditional method.

On the traditional shipyard at Bagan Siapiapi, after the built the ship will be launched into the ocean to estimate capacity and check center of weight. Some people on that area usually using high sinking of ship hull as a reference to define weight of ship, and center of weight define from stability of ship net. This way doesn't accurate so they change a shape and dimension of ship while doing testing.

The habit of community to build a vessel without make a good plan, without a drawing design would be need a long duration to construct of vessel. The center of weight is something important that can be benefits for safety crew and any passenger who boarding it. In the early step designer must be define a point of load at a ship for good stability in shipping [2]. Generally fleets of fishing vessel at Bagan Siapiapi on the operate using a gill net .

Many shipyard in Indonesia still used traditional method on ship manufacture until this day. In fact vessel made by traditional manner can be operate for fishing as well as modern vessel.

However it need some attempt to develop and carry out some modernization on design and manufacture process for traditional shipyard.

This research aims to study capacity and define center of weight of ship net at Bagan Siapiapi.

2.0 LITERATURE REVIEW

2.1 Fishing Vessel

Fishing vessels are vessels that are directly used in fishing operations to pick up fish, animal, or anything plant water [6].Ships in Indonesia are generally made traditionally. Tradition is a hereditary customs (of ancestors) are still running in the community. Generally ship in Indonesia made by traditional method in thinking and acting. This tradition is inherited from ancestors in society until this time.

2.2 Ship Capacity

The capacity of the ship is designed to be sufficient to accommodate fish, fuel, water, engine, accommodation spaces and others room [5]. Thus, the internal capacity of fishing vessels, among other things: the fish hold, engine room, fresh water tank, fuel tank, the accommodation space, and others. Gross ton (GT) is a ship capacity associated with capability of vessel to be loaded.

2.3 Center of Weight

Center of weight is the center of gravity. It's point of working force in down direction. Position of G in the empty vessel define by result from stability experiment, depend on divisions of room on the ship. So as long there are no action to remove, add or reduce a load point of G will not be changed even the ship maneuvering. Figure of 1 explained of specify center gravity.

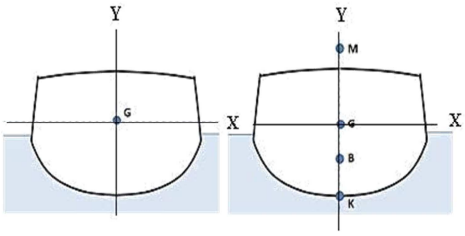

Figure 1: Center of gravity of ship

Notice:

M = point of meta center
K = *Lunas*
B = point of floating

2.4 Stability of Ship

On the fishing process, stability and safety on vessel is main required term to ensure on ship because dangerous environment in many area operation of ship. This is related to characteristic ship operating of crew [4]. Some of requirements on condition to obtain stability in balance are:

1) Floating Force (Fa) = weight force or gravity force (W),
2) Center of floating point and weight point within on the same line,
3) Point of weight of ship define below of meta center line. Figure 2 shows the balance on stable condition of traditional ship model.

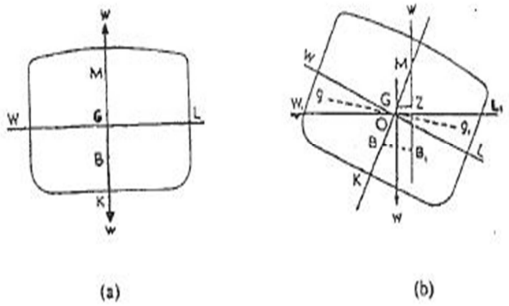

Figure 2: (a) Balance (b) Balance on stable condition

Notice:

B = Floating point
G = Weight point
K = Lunas
M = Point of meta center
W= Weight of ship

3.0 METHODOLOGY

3.1 Density Testing

The density of a substance is ratio between mass with volume of substance. Some mechanical properties of wood is related to specific of weight to describe mass per unit volume. On Figure 3 was shown a flowchart to check out density a substance.

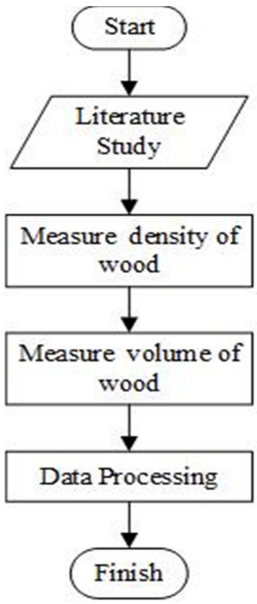

Figure 3: Flowchart testing a density

Table 1: Mass of part of ship net

No	Ship Construction	Quantity	Volume total wood specify	Woods Name	Mass
			(m^3)		(kg)
1	Lunas	1	0.600	Keruwing	540.00
2	Linggi	2	0.380	Resak	340.60
3	Gading-gading	36	0.650	Laban	592.63
4	Balok dek	18	0.380	Keruwing	300.70
5	Badan kapal	1	3.330	Laban	3029.40
6	Landasan mesin	2	0.092	Resak	83.40
7	Putaran Sauh	2	0.040	Laban	37.70
8	Rumah Kapal	1	1.140	Meranti	881.48
9	Box Ikan	1	0.170	Meranti	132.13
10	Mesin	1	-		370.00
			Total		6308.04

Some data would be collected appropriate and systematic such as capacity, point of weight and lay out design about construction of ship. The mass of part of ship net is shown in Table 1. This research was used study case to compare data directly on field or shipyard.
This method was applied to assigning on shipyard at Bagan Siapiapi. Figure 4 was shown flowchart diagram to do it.

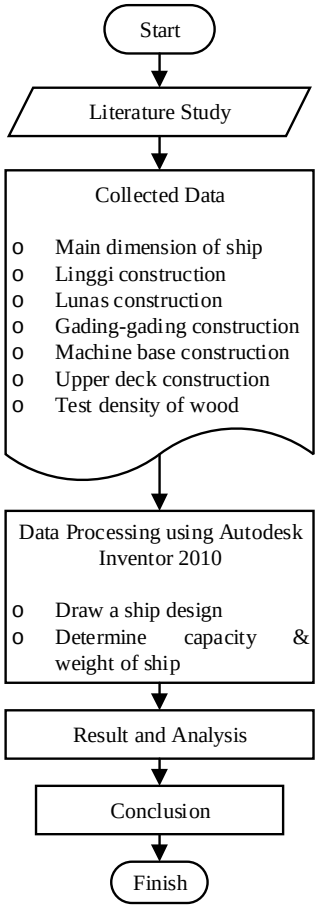

Figure 4: Flowchart of research

4.0 RESULT and DISCUSSION

4.1 Ship Capacity

Mass of the ship net at Bagan Siapiapi shipyard are indicated in Table 1. The ship mass are amount of structure mass construction of ship net

$$W = (\rho_{air\ laut})\ x\ (V_{terendam\ teoritis})\ x\ g$$

$$V_{terendam\ teoritis} = \frac{m_{kapal}}{\rho_{air\ laut}} = \frac{6308.04\ kg}{1025\ {}^{kg}/_{m^3}} = 6.15\ m^3$$

$$\begin{aligned} W &= (\rho_{air\ laut})\ x\ \Delta V\ x\ g \\ &= (\rho_{air\ laut})\ x\ (V_{muatan\ penuh}\ x\ V_{muatan\ kosong\ teoritis})\ x\ g \\ &= 1025\ kg/m^3\ x(13.07\ m^3 - 6.15\ m^3)x\ 9.81\ m/s^2 \\ &= 69582.33\ N = 7093\ kg \end{aligned}$$

$$\begin{aligned} W_{max} &= W_{min}\ x\ W_{muat} \\ &= 6308{,}04\ kg\ x\ 7093\ kg \\ &= 13401.04\ kg \end{aligned}$$

The sinking of ship hull is 870 mm. This data obtained from observed on field at shipyard in Bagan Siapiapi. Actually ship capacity can determine through;

$$\begin{aligned} W_{teoritis} &= (\rho_{air\ laut})\ x\ (V_{muatan\ penuh}\ x\ V_{muatan\ kosong\ teoritis})\ x\ g \\ &= 1025\ kg/m^3\ x(13.07\ m^3 - 6.17\ m^3)x\ 9.81\ m/s^2 \\ &= 69381.23\ N = 7072\ kg \end{aligned}$$

$$\begin{aligned} W_{max} &= W_{min}\ x\ W_{muat} \\ &= 6308.04\ kg\ x\ 7072\ kg \\ &= 13380.04\ kg \end{aligned}$$

4.2 Center of Weight and Point Stability of Ship

Position center of weight of ship was determined using commercial software Autodesk Inventor 2010. Figure 5 shows that the center of weight of ship net. The roll angle related to deep sinking a hull of ship is shown in Table 2.

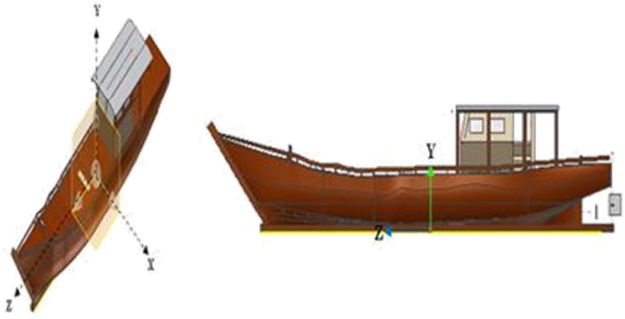

Figure 5: Center of weight of ship net

Empty condition
X = 0.9 mm, Y = 888.5mm, Z = -162.5mm

Full load condition
X = 0.7 mm, Y = 976.7 mm, Z = -600.4 mm

Tabel 2 : Roll angle related to deep sinking a hull of ship.

No	Deep sinking (mm)	Roll angle Front view (^{o})	Roll angle Side view (^{o})
1	823,00	89,24	-84,00
2	860,70	89,38	-81,20
3	898,40	89,50	-81,00
4	936,10	-89,68	-81,90
5	973,80	-89,69	89,00
6	1011,50	-89,74	85,00
7	1049,20	-89,62	80,50
8	1086,90	-89,58	80,30
9	1124,60	-89,63	80,25
10	1162,30	-89,61	80,08
11	1200,00	-89,80	80,03

4.3 Discussion

1.) The depth sinking hull of ship from water level is 870 mm on the condition without load. Autodesk Inventor software shows that condition would be happen if 6.11 m^3 volume of ship submerged. On the other side community on the shipyard at Bagan Siapiapi estimate deep sinking of hull 1200 mm from water level at the full load while on Autodesk Inventor software shown 13.01 m^3 volume ship submerged.

Weight of ship is 13216.6 kg be obtained from calculation whereas real condition maximum weight of ship 13195.6 kg.

There is a difference result between software and real fact amount of 21 kg. Therefore a deep sinking of hull from water level was affected to capacity of load. Capacity of ship net manufactures by shipyard in Bagan Siapiapi is 7.093 kg.

2.) Position center weight of ship net from Autodesk Inventor software 2010 are;

Without load
X = 0.9 mm, Y = 888.5mm, Z = -162.5mm

On full load;
X = 0.7 mm, Y = 976.7mm, Z = -600.4 mm

The result indicates center weight of ship net is affected by working load. In this case the load evenly distributed.

3.) The deep sinking of hull of ship net without load is 823 mm. Roll angle is 89.24 ^{O} and pitch angle is 84^o. The ship would rolling to left and rear. Otherwise deep sinking of hull 1200 mm on the full load and -89,8^o roll angle and 80.03 O at pitch angle while the ship rolling to left and rear.

5.0 CONCLUSION

Capacity ship net at Bagan Siapiapi is 7093 kg and weight at the full load is 13401.04 kg. Position center weight of ship net at Bagan Siapiapi are; X = 0.7 mm, Y = 888.5mm and Z = -162.5 mm. Angle of roll and angle of pitch on the empty load less than full load condition.

REFERENCE

1. Muharam, S.A. 2011. ”Desain Dan Konstruksi Kapal Fibreglass Di PT. Carita Boat Indonesia Kecamatan Setu Kota Tangerang Selatan Banten”. Theses. Department Technology and Management Fisheries IPB.
2. Nofrizal. 1998. ”Konstruksi Kapal Perikanan Trammel Net Di Kecamatan Rangsang Kabupaten Bengkalis Provinsi Riau”. Theses. Department Management Water Resources University of Riau.
3. Umam, Misbahul. 2007. ”Desain dan Konstruksi Kapal Purse Seine Semangat Baru di Galangan Kapal Pulau Tidung”. Theses. Department Degree of Bogor : Faculty of Fisheries IPB.
4. Smith RM. 1975. *Elements of Ship Design*. London: Marine Management (Holding) Ltd. 76 Marj Lane.
5. Tyson, J. 1985. *Design of Small Fishing Vessels*. England: Fishing News Book.
6. Department Fisheries and Marine 2007. Pemeliharaan Perahu dan Kapal Ikan. Fisheries Network Information Jakarta. Indonesia.

Journal of Ocean, Mechanical and Aerospace
-Science and Engineering-, Vol.24

October 30, 2015

Study on Structural Deflection in Attitude Maneuvers of Flexible Satellite Equipped with Fuel-Efficient Input Shaper

Setyamartana Parman[a,*]

[a)]*Department of Mechanical Engineering, Universiti Teknologi PETRONAS, Bandar Seri Iskandar, Perak, Malaysia*

*Corresponding author: setyamartana@petronas.com.my

Paper History

Received: 16-October-2015
Received in revised form: 27-October-2015
Accepted: 29-October-2015

ABSTRACT

Input shaping technique can successfully suppresses residual vibration in slew maneuvers of flexible systems. This paper studies transient structural deflections of flexible satellite during attitude maneuvers controlled using input shaper. The satellite consists of a rigid main body and two symmetrical flexible solar panels. The equations of motion of the satellite are derived using Lagrange's formulation, and elastic motions of flexible structures are discretized following the finite element method. The attitude maneuvers are equipped with on-off constant amplitude inputs. For fast maneuver, the satellite has poor accuracy after the maneuver. To resolve this issue, input shaper is applied to maneuver the satellite. Various fuel-efficient shaped inputs are studied in order to conclude the relation of input shape and transient maximum deflection resulted.

KEY WORDS: *Fuel-Efficient; Input Shaper; Flexible Satellite; Finite Element; Attitude Maneuver*.

LIST OF SYMBOLS

r	Translational Displacement of Main Body
d	Displacement Vector of Flexible Substructures
Θ	Rotational Displacement of Main Body
ϕ	Roll Angle
θ	Pitch Angle
ψ	Yaw Angle
$\boldsymbol{\omega}_0$	Angular Velocity of Satellite Orbit
m	Total Mass of Satellite
$\mathbf{I}$	Total Inertia Matrix of Satellite
Q	Coupling Matrix between Translational and Rotational Motions of Main Body
$\mathbf{W}$	Coupling Matrix between Translational Motion of Main Body and Flexible Substructures Displacement
$\mathbf{A}$	Coupling Matrix between Rotational Motion of Main Body and Flexible Substructures Displacement
$\mathbf{M}$	Mass Matrix of Flexible Substructures
$\mathbf{K}$	Stiffness Matrix of Flexible Substructures
A_i, t_i	Amplitudes and Time Locations of Input Shaper
$\mathbf{F}_b$, $\mathbf{T}_b$	Control Forces and Torques Acting on Main Body
$\mathbf{F}_a$	External Forces and Torques Acting on Flexible Substructures
f	Number of Degrees of Freedom of Flexible Substructures

1.0 INTRODUCTION

A satellite or satellite in operation needs certain accuracies in its attitude. To keep the orientation, the satellite during its operation in space requires frequent corrections of its attitude. Attitude maneuver of rigid satellite can be done without a lot of vibration problems after reaching its desired attitude. For the flexible satellite maneuvering the attitude without regard to system flexibility or without controls on the flexible members, large amplitude transient and steady state oscillations may occur, especially when the system is equipped with on-off jets. Such a system often needs a rest-to-rest attitude maneuver with small vibration both during and at the end of the maneuver. For example, it may be necessary to generate a torque profile such that the satellite is rotated through a desired attitude angle, while the deflections of flexible members remain small throughout the maneuver and go to zero at the end of the maneuver.

To minimize modal vibration in a flexible satellite system, which is equipped with on-off reaction jets, the input shaping methods have been developed [1]. Parman and Koguchi [2-6] demonstrate an application of shaped commands to maneuver attitudes of a flexible satellite with a large number of flexible modes. They show that the resultant vibrations can be reduced drastically when the satellite is subjected to shaped inputs suppressing the vibration at the frequency with largest vibration amplitude. However, the structural deflections of the satellite are still large enough.

To resolve large transient deflection during the maneuver using input shaper, several researchers formulated analytical approximation to be included in the input shaping constraints [7-8]. They used a simple model of two masses connected with a spring and selected a simple configuration of input shape. For this kind of study, the analytical formulation of the input constraints can be easily defined. When the system is having a lot of flexible modes, such as finite element model of flexible satellite, analytical equations in limiting deflections of flexible members become very complicated and impossible to be formulated.

This paper presents computer simulations of attitude maneuvers of a satellite with flexible solar panels equipped with constant-amplitude thrusters. The finite element model of satellite developed by Parman [2, 4-5] is used. The study investigates a condition of the satellite where offset angle of the solar panels is 30°. For this setting angle, there is a coupling motion between roll and yaw displacements of the satellite. The problem appearing in fast maneuver of the satellite under constant-amplitude input is introduced first. Then, fuel-efficient input shapers are applied to overcome the issue. Various results of shaped input are simulated and compared to study the influence of fuelling pulse duration to the solar panel's deflection during transient response.

2.0 A SATELLITE WITH SYMMETRICAL FLEXIBLE SOLAR PANELS

The particular satellite investigated in this study is a satellite consisting a main body and two symmetrical solar panels, as shown in Fig. 1. The main body is a rigid cuboid. To identify the satellite attitude relative to an inertial frame $F_i(O_iX_iY_iZ_i)$, a main body fixed frame $F_b(O_bX_bY_bZ_b)$ is defined. The solar panels are large and long in sizes and they are supposed as flexible structures. To discretize elastic deformations of the panels, the finite element method (FEM) is used. For this application, each solar panel is divided into 32 rectangular bending plate elements. The elements on the right side are numbered from 1 to 16 and on the left side from 17 to 32, while their nodal points are numbered from 1 to 27 and from 28 to 54. Substructure reference frames $F_j(O_jX_jY_jZ_j)(j = 1, 2, \cdots, 32)$ are defined to measure displacements of their nodes. The Y_j-axes ($j = 1, 2, \cdots, 16$) of the right side panel are parallel to the Y_b-axis, while the Y_j-axes ($j = 17, 18, \cdots, 32$) of the left side are anti-parallel. All Z_j-axes are normal to their panels. The origin of the main body fixed frame O_b is placed on the mid-point of the longitudinal axis of the solar panels. The solar panels are oriented towards the sun, and the declination with respect to the X_b-axis is identified by the offset angle δ.

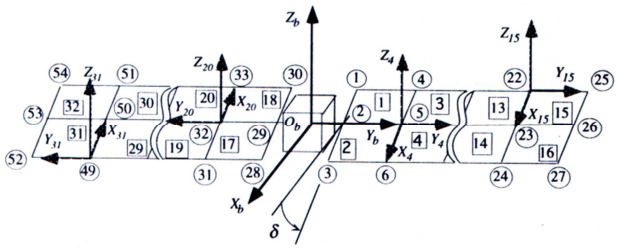

Figure 1: The finite element model of flexible satellite

The attitude angles of the satellite are expressed in Bryant's angles: roll angle ϕ, pitch angle θ, and yaw angle ψ; where the definition of these angles can be seen in Fig. 2. In this figure, $F_o(X_oY_oZ_o)$ is the satellite orbital frame.

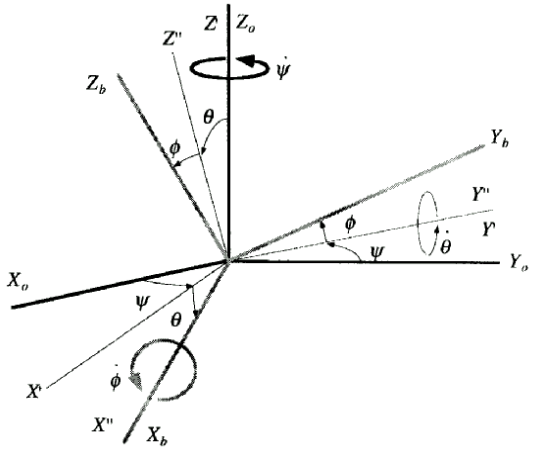

Figure 2: The rotations from observation reference frame F_o to main body-fixed reference frame F_b

2.1 Mathematical Model of Flexible Satellite Dynamics

In this study, equations of motion of general gravity oriented and non-spinning flexible satellite dynamics are derived using a Lagrange's formulation following the works of Parman [2, 4-5]. For this purpose, the expressions of kinetic energy and potential energy for the whole satellite need to be determined first. Since the satellite considered consists of the rigid main body and two flexible solar panels, the kinetic energy and potential energy of the satellite can be formulated by observing the rigid body and flexible solar panels separately. After that, the total satellite kinetic and potential energies can be defined by summing the resulted kinetic and potential energies at above.

2.1.1 Kinetic energy.

The kinetic energy of the rigid main body of the satellite can be written in the following form:

$$E_{kb} = \frac{1}{2}\dot{\mathbf{r}}_{i,b}^T\dot{\mathbf{r}}_{i,b}m_b + \frac{1}{2}\boldsymbol{\omega}_{b,i}^T\mathbf{I}_b\boldsymbol{\omega}_{b,i} + \frac{1}{2}\dot{\mathbf{r}}_{i,b}^T\mathbf{Q}_b\boldsymbol{\omega}_{b,i} \quad (1)$$

where $\mathbf{r}_{i,b}$ is a vector from O_i to O_b (see Fig. 3) with the overdot, ($\dot{}$) indicating its differentiation with respect to time relative to F_i,

$\boldsymbol{\omega}_{b,i}$ is the angular velocity vector of F_b relative to F_i, m_b is the total mass of the main body, $\mathbf{I}_b$ is the inertia matrix of the body relative to O_b, and $\mathbf{Q}_b$ is the coupling matrix between translational and rotational displacements of the main body. If O_b coincides with the center of mass of the main body, the value of $\mathbf{Q}_b$ equals zero.

The kinetic energy of flexible solar panels can be written in the following form:

$$E_{ka} = \frac{1}{2}\dot{\mathbf{r}}_{i,b}^T\dot{\mathbf{r}}_{i,b}m_a + \frac{1}{2}\dot{\mathbf{d}}^T\mathbf{M}\dot{\mathbf{d}} + \frac{1}{2}\boldsymbol{\omega}_{b,i}^T\mathbf{I}_a\boldsymbol{\omega}_{b,i} + \boldsymbol{\omega}_{b,i}^T\mathbf{A}\dot{\mathbf{d}} + \dot{\mathbf{r}}_{i,b}^T\mathbf{W}\dot{\mathbf{d}} + \dot{\mathbf{r}}_{i,b}^T\mathbf{Q}_a\boldsymbol{\omega}_{b,i} \quad (2)$$

where $\mathbf{d}$ is the displacement vector of flexible solar panels, m_a is the mass of solar panels, $\mathbf{M} = \sum_{j=1}^{N}\mathbf{P}_j^T\mathbf{M}_j\mathbf{P}_j$ is their mass matrix, and $\mathbf{I}_a = \sum_{j=1}^{N}\mathbf{T}_j^T\mathbf{I}_j\mathbf{T}_j$ is their inertia matrix with respect to O_b. The coupling matrices $\mathbf{A} = \sum_{j=1}^{N}\mathbf{T}_j^T\mathbf{A}_j\mathbf{P}_j$ and $\mathbf{W} = \sum_{j=1}^{N}\mathbf{T}_j^T\mathbf{W}_j\mathbf{P}_j$ relate the main body rotational and translational displacements, respectively, to the solar panel displacements, while $\mathbf{Q} = \sum_{j=1}^{N}\mathbf{T}_j^T\mathbf{Q}_j\mathbf{T}_j$ is the coupling matrix between the translational and rotational displacements of the main body contributed by the undeform-state solar panels. In these matrices, N is the number of elements of flexible solar. For the jth element, $\mathbf{T}_j$ is the transformation matrix from F_b to F_j, $\mathbf{P}_j$ is the assembling matrix relating the element displacement vector $\boldsymbol{d}_j$ and the displacement vector of flexible solar panels $\mathbf{d}$ in the form of $\mathbf{d}j = \mathbf{P}_j\,\mathbf{d}$, $\mathbf{M}_j = \int_{mj}\mathbf{C}_j^{\mathrm{T}}\mathbf{C}_j\,dm$ is the mass matrix, $\mathbf{A}_j = {}^j\tilde{\mathbf{r}}_{b,o}\mathbf{W}_j + \int_{m_j}{}^j\tilde{\mathbf{r}}_{o,p_0}\mathbf{C}_j\,dm$ are the coupling matrices between rotational and translational displacements of the main body respectively and the element displacements, $\mathbf{Q}_j = \int_{m_j}({}^j\tilde{\mathbf{r}}_{b,o} + {}^j\tilde{\mathbf{r}}_{o,p_0})^T\,dm$ is the coupling matrix for the translational and rotational displacements of the main body contributed by the undeform-state element, and $\mathbf{I}_j = \int_{m_j}({}^j\tilde{\mathbf{r}}_{b,o} + {}^j\tilde{\mathbf{r}}_{o,p_0})^T({}^j\tilde{\mathbf{r}}_{b,o} + {}^j\tilde{\mathbf{r}}_{o,p_0})dm$ is the element inertia matrix with respect to O_b. $\mathbf{C}_j$ is the element shape function matrix, ${}^j\mathbf{r}_{b,o}$ and ${}^j\mathbf{r}_{o,p0}$ are vectors from O_b to O_j and from O_j to a particle p with mass dm of the element in the undeform state respectively expressed in F_j, while a general notation of (˜) means the skew symmetric matrix of a prescribed vector.

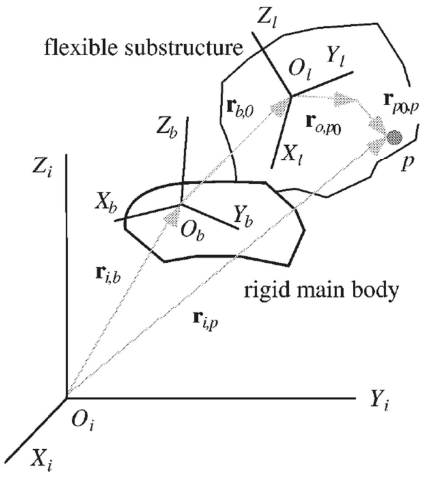

Figure 3: Position vectors from $F_i(X_iY_iZ_i)$ to a particle p

2.1.2 Potential Energy

The potential energy of the satellite consists of the potential energy of its undeform state and the potential energy due to elastic deformations of flexible solar panels. The potential energy of the undeform state, in this study, is measured relative to the earth. When the satellite orbit is circular, it can be expressed as

$$E_{pr} = E_{pr}(\mathbf{r}_{i,b}) \quad (3)$$

The potential energy due to elastic deformations is the sum of the strain energy of flexible substructures and the potential energy due to external forces acting on the substructures with a minus sign. By following the general finite element method procedures, the potential energy due to the elastic deformations of flexible solar panels can be written in the following form:

$$E_{pa} = \tfrac{1}{2}\,\mathbf{d}^{\mathrm{T}}\,\mathbf{K}\,\mathbf{d} + \mathbf{d}^{\mathrm{T}}\,\mathbf{F}_a \quad (4)$$

where $\mathbf{K} = \sum_{j=1}^{N}\mathbf{P}_j^T\,\mathbf{K}_j\mathbf{P}_j$ is the stiffness matrix of the solar panels and $\mathbf{F}_a = \sum_{j=1}^{N}\mathbf{P}_j^T\mathbf{f}_j$ is the discrete external forces vector acting on the solar panels. For the jth element, $\mathbf{f}_j = \int_{V_j}\mathbf{C}_j^T\,\mathbf{F}_f\,dV$ is the discrete external forces vector acting on the nodes and $\mathbf{K}_j = \int_{V_j}\mathbf{C}_j^T\,\mathbf{B}_j^T\mathbf{R}_j\mathbf{B}_j\mathbf{C}_j\,dV$ is the stiffness matrix. $\mathbf{F}_f$ is a distributed external forces vector working on the element, $\mathbf{B}_j$ is an operator matrix containing first or second order derivative operators, and $\mathbf{R}_j$ is an elasticity matrix of element j.

2.1.3 Full model equations of motion of flexible satellite

To derive the equations of motion by following Lagrangian procedure, the Lagrangian operator, $L = E_k - E_p$, and Lagrange's equations of motion, $\frac{d}{dt}\left(\frac{\partial L}{\partial \dot{\mathbf{q}}}\right) - \frac{\partial L}{\partial \mathbf{q}} + \frac{\partial S}{\partial \dot{\mathbf{q}}} = \mathbf{F}$ are used. In these expressions, $E_k = E_{ka} + E_{kb}$ is the satellite total kinetic energy, $E_p = E_{pa} + E_{pr}$ is the satellite total potential energy, $\mathbf{q}$ is the satellite general displacement vector, $\mathbf{F}$ is the general external forces vector working on the satellite, $S = \frac{1}{2}\dot{\mathbf{q}}^T\mathbf{D}\dot{\mathbf{q}}$ is the satellite Rayleigh's dissipation, where $\mathbf{D}$ is the satellite damping matrix. Then, it is considered that control (external) forces acting on the rigid main body of the satellite are much larger than the forces resulting from the potential energy of the undeform state. For simplicity, $\boldsymbol{\omega}_{b,i}$ and $\mathbf{r}_{i,b}$ then will be written as $\boldsymbol{\omega}$ and $\mathbf{r}$ only, respectively, in this paper.

By using Eqs. (1)-(4), the equations of motion of the satellite can then be linearized and written as follows:

$$\begin{bmatrix} m\mathbf{U}_3 & \mathbf{Q} & \mathbf{W} \\ \mathbf{Q}^T & \mathbf{I} & \mathbf{A} \\ \mathbf{W}^T & \mathbf{A}^T & \mathbf{M} \end{bmatrix}\begin{Bmatrix} \ddot{\mathbf{r}} \\ \ddot{\boldsymbol{\Theta}} \\ \ddot{\mathbf{d}} \end{Bmatrix} + \begin{bmatrix} \mathbf{0}_{3\times3} & \mathbf{Q}\tilde{\boldsymbol{\omega}}_0 & \mathbf{0}_{3\times f} \\ \mathbf{0}_{3\times3} & \mathbf{I}\tilde{\boldsymbol{\omega}}_0 & \mathbf{0}_{3\times f} \\ \mathbf{0}_{f\times3} & \mathbf{A}^T\tilde{\boldsymbol{\omega}}_0 & \mathbf{D} \end{bmatrix}\begin{Bmatrix} \dot{\mathbf{r}} \\ \dot{\boldsymbol{\Theta}} \\ \dot{\mathbf{d}} \end{Bmatrix} + \begin{Bmatrix} \mathbf{0}_3 \\ \mathbf{0}_3 \\ \mathbf{K}\mathbf{d} \end{Bmatrix} = \begin{Bmatrix} \mathbf{F}_b \\ \mathbf{T}_b \\ \mathbf{F}_a \end{Bmatrix} \quad (5)$$

In Eq. (5), m is the total mass of the satellite, $\mathbf{Q}$ is the total coupling matrix for the translational and rotational displacements of the rigid main body, $\mathbf{W}$ is the total coupling matrix for the translational displacements of the rigid main body and the displacements of flexible solar panels, $\mathbf{I}$ is the total inertia matrix, $\mathbf{A}$ is the total coupling matrix for the rotational displacements of the rigid main body and the displacements of flexible solar panels. The $\mathbf{M}$, $\mathbf{D}$ and $\mathbf{K}$ are the mass, damping and stiffness matrices of the flexible solar panels, respectively. The $\tilde{\boldsymbol{\omega}}_0$ is the skew symmetric matrix of angular velocity of the satellite orbit

$\boldsymbol{\omega}_0$, $\mathbf{r}$ is the translational displacement of the rigid main body, $\boldsymbol{\Theta}$ is the rotational displacement of the rigid main body which is expressed in a vector of Bryant's angles, and $\mathbf{d}$ is the displacements of the flexible solar panels. $\mathbf{F}_b$ and $\mathbf{T}_b$ are external forces and torques vectors acting on the rigid main body, $\mathbf{F}_a$ is the vector of external forces and torques acting on the solar panels, while f is the total number of degrees of freedom of the solar panels. In this paper, the flexible structural subsystems are supposed to have no dissipation properties, so that $\mathbf{D} = \mathbf{0}$.

2.2 Solar Panels as a Collection of Rectangular Plate Elements

The equations of motion of general satellite have been formed in Eq. (5). To use this equation, the mass and stiffness matrices need to be evaluated for a particular flexible substructure discretization. In this paper, the attitude of the hypothetical satellite is chosen as follows: the Z_b-axis should point to the centre of earth, the Y_b-axis is normal to the orbital plane, and the X_b-axis should point to the satellite linear velocity when there are no attitude errors. For the application of finite element method to discretize elastic deformations of solar panels, the following idealizations are used:

(a) The solar panels are divided into rectangular flat plate bending elements.
(b) Each element has a uniform mass density.
(c) Only out-of-plane deformations of solar panels are considered.
(d) External loads (both forces and torques) on the solar panels are assumed to work on the nodal points of the elements.
(e) The Y_l-axes of elements and the Y_b-axis of main body frame are parallel or antiparallel (see Fig. 1). The X_l-axes and Y_l-axes of elements are in the panel plane, and their Z_l-axes are normal to the plane.

By using the above idealizations, each element of solar panel has 12 degrees of freedom in total, as shown by Fig. 4. Also, the material of solar panels are assumed as isotropic materials. For an isotropic plate, $\mathbf{R}_j$ can be written as

$$R_j = \frac{Ec^3}{12(1-\nu^2)}\begin{bmatrix} 1 & \nu & 0 \\ \nu & 1 & 0 \\ 0 & 0 & \frac{1-\nu}{2} \end{bmatrix} \tag{6}$$

where E, c and ν are the Young's modulus, thickness, and Poisson's ratio of j-th element, respectively.

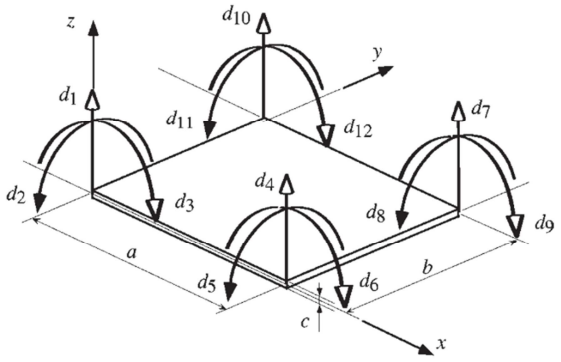

Figure 4: A rectangular plate element model of solar panel with out-of-plane displacement.

The shape function matrix introduced by Bogner [9] is selected. This shape function matrix can guarantee that deflections and slopes are all continuous on the edge of the element, and its expression for the j-th element is as follows:

$$\mathbf{C}_j^T = \begin{bmatrix} (1+2\xi)(1-\xi)^2(1+2\eta)(1-\eta)^2 \\ (1+2\xi)(1-\xi)^2\eta(1-\eta)^2 b \\ -\xi(1-\xi)^2(1+2\eta)(1-\eta)^2 a \\ (1+2\xi)(1-\xi)^2(3-2\eta)\eta^2 \\ -(1+2\xi)(1-\xi)^2(1-\eta)\eta^2 b \\ -\xi(1-\xi)^2(3-2\eta)\eta^2 a \\ (3-2\xi)\xi^2(3-2\eta)\eta^2 \\ -(3-2\xi)\xi^2(1-\eta)\eta^2 b \\ (1-\xi)\xi^2(3-2\eta)\eta^2 a \\ (3-2\xi)\xi^2(1+2\eta)(1-\eta)^2 \\ (3-2\xi)\xi^2\eta(1-\eta)^2 b \\ (1-\xi)\xi^2(1+2\eta)(1-\eta)^2 a \end{bmatrix} \tag{7}$$

where a and b are the length and width of element, respectively, $0 \le (\xi = x/a) \le 1$, and $0 \le (\eta = y/b) \le 1$. For this shape function matrix, the coupling matrix $\mathbf{A}j$ can be obtained as follows:

$$\mathbf{A}_j^T = \frac{\rho abc}{24}\begin{bmatrix} 6y_{0_j} + \frac{9}{5}b & -6x_{0_j} - \frac{9}{5}a & 0 \\ by_{0_j} + \frac{2}{5}b^2 & -bx_{0_j} - \frac{3}{10}ab & 0 \\ -ay_{0_j} - \frac{3}{10}ab & ax_{0_j} + \frac{2}{5}a^2 & 0 \\ 6y_{0_j} + \frac{21}{5}b & -6x_{0_j} - \frac{9}{5}a & 0 \\ -by_{0_j} - \frac{3}{5}b^2 & bx_{0_j} + \frac{3}{10}ab & 0 \\ -ay_{0_j} - \frac{7}{10}ab & ax_{0_j} + \frac{2}{5}a^2 & 0 \\ 6y_{0_j} + \frac{21}{5}b & -6x_{0_j} - \frac{21}{5}a & 0 \\ -by_{0_j} - \frac{3}{5}b^2 & bx_{0_j} + \frac{7}{10}ab & 0 \\ ay_{0_j} + \frac{7}{10}ab & -ax_{0_j} - \frac{3}{5}a^2 & 0 \\ 6y_{0_j} + \frac{9}{5}b & -6x_{0_j} - \frac{21}{5}a & 0 \\ by_{0_j} + \frac{2}{5}b^2 & -bx_{0_j} - \frac{7}{10}ab & 0 \\ ay_{0_j} + \frac{3}{10}ab & -ax_{0_j} - \frac{3}{5}a^2 & 0 \end{bmatrix} \tag{8}$$

where x_{0j} and y_{0j} are the components of ${}^l\mathbf{r}_{b,o}$ for the j-th element along its X_l and Y_l-axes, respectively (see Figs. 1 and 3), ρ is the mass density, while the inertia matrix $\mathbf{I}_j$ can be written as follows:

$$\mathbf{I}_j = \rho abc\begin{bmatrix} I_{j_{11}} & I_{j_{21}} & I_{j_{31}} \\ I_{j_{21}} & I_{j_{22}} & I_{j_{32}} \\ I_{j_{31}} & I_{j_{32}} & I_{j_{33}} \end{bmatrix} \tag{9}$$

where

$$I_{j_{11}} = y_{0_j}^2 + \tfrac{1}{12}c^2 + \tfrac{1}{3}b^2 + y_{0_j}b,$$
$$I_{j_{21}} = -\tfrac{1}{2}\left(\tfrac{1}{2}ab + y_{0_j}a + x_{0_j}b\right) - x_{0_j}y_{0_j},$$
$$I_{j_{31}} = I_{j_{32}} = 0,$$
$$I_{j_{22}} = x_{0_j}^2 + \tfrac{1}{12}c^2 + \tfrac{1}{3}a^2 + x_{0_j}a,$$
$$I_{j_{33}} = x_{0_j}^2 + y_{0_j}^2 + \tfrac{1}{3}\left(a^2 + b^2\right) + x_{0_j}a + y_{0_j}b,$$

and the coupling matrix for rotational displacements of the main body and the displacements of element j can be written as follows:

$$\boldsymbol{W}_j = \frac{\rho abc}{24}\begin{bmatrix} 0 & 0 & 0 & 0 & 0 & 0 & 0 & 0 & 0 & 0 & 0 & 0 \\ 0 & 0 & 0 & 0 & 0 & 0 & 0 & 0 & 0 & 0 & 0 & 0 \\ 6 & b & -a & 6 & -b & -a & 6 & -b & a & 6 & b & a \end{bmatrix} \quad (10)$$

3.0 PROBLEM IN FAST ATTITUDE MANEUVERS USING CONSTANT-AMPLITUDE INPUTS

In this study, it is supposed that the satellite has no control and no damping properties on the flexible solar panels. The control inputs for attitude maneuvers are only torques applied to the satellite's rigid main body, as results of on-off reaction jets of the thruster in constant amplitude. For such a system, the attitude angle acceleration of satellite as a rigid body motion can be written as

$$\begin{Bmatrix} \ddot{\phi} \\ \ddot{\theta} \\ \ddot{\psi} \end{Bmatrix} = \begin{bmatrix} I_{xx} & I_{xy} & I_{xz} \\ I_{xy} & I_{yy} & I_{yz} \\ I_{xz} & I_{yz} & I_{zz} \end{bmatrix}^{-1} \begin{Bmatrix} T_{b_x} \\ T_{b_y} \\ T_{b_z} \end{Bmatrix} \quad (11)$$

where I_{xx}, I_{yy}, I_{zz}, I_{xy}, I_{xz}, and I_{yz} are components of the inertia matrix **I** of the whole satellite, and T_{bx}, T_{by}, and T_{bz} are components of the torque input vector $\mathbf{T}_b$ on the rigid main body. Integrating Eq. (11) with respect to time results the desired attitude angle velocity,

$$\begin{Bmatrix} \dot{\phi}_d \\ \dot{\theta}_d \\ \dot{\psi}_d \end{Bmatrix} = \int \begin{bmatrix} I_{xx} & I_{xy} & I_{xz} \\ I_{xy} & I_{yy} & I_{yz} \\ I_{xz} & I_{yz} & I_{zz} \end{bmatrix}^{-1} \begin{Bmatrix} T_{b_x} \\ T_{b_y} \\ T_{b_z} \end{Bmatrix} dt \quad (12)$$

and integrating once more gives a desired roll angle displacement,

$$\begin{Bmatrix} \phi_d \\ \theta_d \\ \psi_d \end{Bmatrix} = \int\int \begin{bmatrix} I_{xx} & I_{xy} & I_{xz} \\ I_{xy} & I_{yy} & I_{yz} \\ I_{xz} & I_{yz} & I_{zz} \end{bmatrix}^{-1} \begin{Bmatrix} T_{b_x} \\ T_{b_y} \\ T_{b_z} \end{Bmatrix} dtdt \quad (13)$$

In the simulations, the main body of satellite is supposed to consist of six lumped masses at certain positions with respect to the satellite's center of mass. Values and positions of the lumped masses are listed in Table 1. Table 2 mentions parameters of satellite's flexible solar panels used in the computer simulations.

Table 1: Lumped masses consisting of the rigid main body

Mass (kg)	Position (m)		
	x_b	y_b	z_b
400	0.40	0.00	0.00
400	-0.40	0.00	0.00
500	0.00	0.50	0.00
500	0.00	-0.50	0.00
550	0.00	0.00	1.40
550	0.00	0.00	-1.40

Table 2: Parameters of the solar panels of satellite

Description	Values
Number of solar panels	2
Dimension of each solar panel (m^3)	12 x 2.4 x 0.03
Young's modulus, E (N/m^2)	0.6×10^8
Poisson ratio, ν	0.3
Mass density, ρ (kg/m^3)	120
Number of elements in each solar panel	16
Dimension of each element, b x a x c, m^3	1.5 x 1.2 x 0.03
Offset angle, δ (degrees)	30
Distance between panel's root and O_b, m	1.80

As the boundary condition for the model, the roots of solar panels are always in the straight lines. There are no deflections for the panel's roots from time to time. It means that $\mathbf{d}_1$, $\mathbf{d}_2$, $\mathbf{d}_3$, $\mathbf{d}_{28}$, $\mathbf{d}_{29}$ and $\mathbf{d}_{30}$ –those are components of **d** in Eq. (5)– are all zero. Be noted that components of **d** are measured in their respective local reference frames. This boundary condition is to represent the real fact that the roots of panels are usually strengthened using the bars or frames, those are relatively rigid, and then connected to the rigid main body using revolve joints.

For this configuration, the origin of the rigid main body fixed reference frame coincides with the centre of mass of the whole satellite in the undeform state, I_{xx} = 17,731 kg·m^2, I_{yy} = 2,580 kg·m^2, I_{zz} =15,557kg·m^2, I_{xy} = I_{yz} =0, and I_{xz} = 43 kg·m^2. At initial the satellite is at undeform condition, while the main body fixed frame and the orbital reference frame coincide with the inertial reference frame. The orbital frame, F_o rotates with respect to the inertial frame, F_i in constant angular velocity

$$\boldsymbol{\omega}_o = -\omega_o \mathbf{j}_i \quad (14)$$

where $\mathbf{j}_i$ is the unit vector in Y_i-axis direction, ω_o = 7.29 × 10^{-5} rad/s, so that F_o performs in F_i one rotation per sidereal day (24 hours of sidereal time or 23 hours 56 minutes 4.09054 seconds of mean solar time). The satellite is at rest condition with attitude angles of -3° in roll, 0° in pitch and 2° in yaw at initial. The attitude will be maneuvered to the nominal operational attitude of geostationary satellite, i.e. roll, pitch and yaw angles are all 0°.

Then, it is supposed that the amplitude of torques in roll, pitch and yaw directions resulted by satellite's thruster are all 8 N-m. The shortest time duration torques of a series of alternating-sign constant-amplitude pulses to maneuver the satellite from one rest to other rest conditions is a bang-bang in maximum amplitude. The bang-bang input for these maneuvers will be two sequence pulses in the alternating sign in the same width. Under this limitation of torque, the profile of bang-bang torques needed consist of 21.528 seconds long of T_{bx} and 16.444 seconds long of T_{bz} bang-bangs. The satellite is subjected to the bang-bang roll and yaw torques simultaneously. Under these inputs, the roll and yaw angles change to the desired angular displacements, while pitch angle is not disturbed. After the torques were removed the roll and yaw angles still oscillate in large amplitudes. The dominant period for these oscillations is 18.7 seconds. This period is relating to the satellite's natural frequency resulted in calculation of 0.3354 rad/s. The total amplitude of residual oscillation is more than 3.6° for roll angle, as shown in Fig. 5(a), and more than 1.4° for yaw angle. The amplitudes of these residual attitude angle oscillations are greater than the desired attitude angle displacements. Such residual oscillations of course are very unacceptable for the precise-oriented satellite. As the attitude angles oscillate, the solar panels also vibrate. The largest residual

vibrations on solar panels happen at their tips. The node 25 experiences unlikely local vertical vibration with high deflection amplitude of 1.46 meters, as shown in Fig. 5(b). Compared with solar panel's length of 12 m, this deflection is about 12 %.

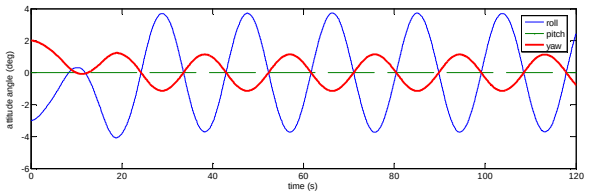

(a)

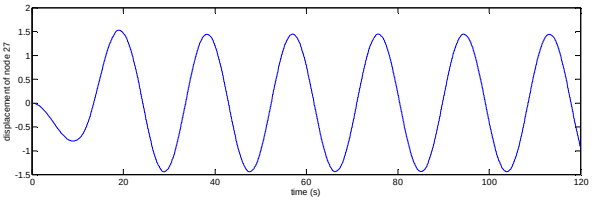

(b)

Figure 5: Time responses under the bang-bang and yaw torque inputs: (a) attitude angle displacement of the main body, (b) vertical displacement of node 25 of solar panel measured in local reference frame

4.0 FUEL-EFFICIENT INPUT SHAPER FOR ATTITUDE MANEUVERS OF FLEXIBLE SATELLITE

A suitable torque input to maneuver the flexible satellite into the desired attitude angle with small or without residual vibration can be 'shaped'. The method is referred to as input shaping. In this method, amplitudes and time locations of the exciting input are determined by solving a set of constraint equations, for example:

(a) constraints on the impulse amplitudes,
(b) constraints on the rigid body motion,
(c) residual vibration constraints, and
(d) fuelling pulses duration.

The flexible satellite studied here is equipped with on-off reaction jets, so it cannot produce variable amplitude actuation thrust; the satellite must be maneuvered with constant amplitude torque pulses. For rest-to-rest maneuvers, the input must contain both positive and negative pulses so that the satellite can be accelerated and then decelerated back to zero velocity. If the number of impulse in shaping the input is selected as 8, the series of alternating-sign pulses for rest-to-rest fuel-efficient maneuver can be generated by convolving a step with an input shaper of the form [1]

$$\begin{bmatrix} A_i \\ t_i \end{bmatrix} = \begin{bmatrix} 1 & -1 & 1 & -1 & -1 & 1 & -1 & 1 \\ t_1 & t_2 & t_3 & t_4 & t_5 & t_6 & t_7 & t_8 \end{bmatrix} \quad (15)$$

In the fuel-efficient commands generated by equation (15), the fuelling periods happen at t_1-t_2, t_3-t_4, t_5-t_6, and t_7-t_8; and the non-fuelling period at t_2-t_3, t_4-t_5 , and t_6-t_7. It means that the command consists of two positive pulses and then is continued with two negative pulses. However, it is selected that the switching times from positive to negative pulses are at the same location, i.e. $t_4 = t_5$ in this paper. Equation (15) becomes the first constraint, i.e. the constraint on impulse amplitudes. Equations (12)-(13) become the second constraints; in this study, the desired attitude angle velocity is $\{0 \;\; 0 \;\; 0\}^T$ deg/s and the desired attitude angle displacement is $\{3° \;\; 0° \;\; -2°\}^T$. The third constraint, the residual vibration at $\omega = 0.3354$ rad/s, the natural frequency with strongest vibration, is set to be smaller than 0.01%,

$$V(\omega) = \sqrt{\frac{\left[\sum A_i \sin(\omega t_i)\right]^2 + \left[\sum A_i \cos(\omega t_i)\right]^2}{\left[\sum A_{bbj} \sin(\omega t_{bbj})\right]^2 + \left[\sum A_{bbj} \cos(\omega t_{bbj})\right]^2}} < 0.01\% \quad (16)$$

where A_{bbj} and t_{bbj} describe the input shaper corresponding to the bang-bang and are given by

$$\begin{bmatrix} A_{bbj} \\ t_{bbj} \end{bmatrix} = \begin{bmatrix} 1 & -2 & 1 \\ t_1 & t_2 & t_3 \end{bmatrix} \quad (17)$$

A lot of shaped inputs will be resulted by using the above three constraints. The fourth constraint is the length of pulses duration. Three cases are selected due to the pulses duration of the roll and yaw torque inputs. These three cases are listed in Table 3. In these selected inputs, each input has about similar duration length in fuelling pulses.

Table 3: Time location of impulses for shaping the torque inputs

	Pulses duration	t_1 **(s)**	t_2 **(s)**	t_3 **(s)**	t_4 **(s)**
Case 1	Roll, 1.2–1.3 s	0	1.204	46.834	48.074
	Yaw, 1.1–1.2 s	0	1.152	28.112	29.302
Case 2	Roll, 1.9–2.1 s	0	1.904	28.104	30.214
	Yaw, 2.7–2.8 s	0	2.782	9.372	12.152
Case 3	Roll, 4.2-4.3 s	0	4.284	9.364	13.584
	Yaw, 2.7-2.8 s	0	2.782	9.372	12.152

	t_5 **(s)**	t_6 **(s)**	t_7 **(s)**	t_8 **(s)**
Case 1	48.074	49.314	94.944	96.148
	29.302	30.492	57.452	58.604
Case 2	30.214	32.324	58.524	60.428
	12.152	14.932	21.522	24.304
Case 3	13.584	17.804	22.884	27.168
	12.152	14.932	21.522	24.304

5.0 SIMULATION OF FLEXIBLE SATELLITE ATTITUDE MANEUVERS USING FUEL-EFFICIENT INPUT SHAPER

The simulation results of Cases 1, 2 and 3 are shown in Figs. 6, 7 and 8, respectively. We can see in Figs. 6(a), 7(a) and 8(a) that under the application of shaped inputs, the attitude angles of the satellite can be brought to zero degree successfully to all cases. The residual oscillation of attitude angle at $\omega = 0.3354$ rad/s can be removed, but another oscillations at higher natural frequencies may occur. However, oscillation suppression at other frequencies is not designated in this paper. The paper focuses on the transient deflections of the flexible solar panels.

Case 1, where the lengths of pulses duration in roll and yaw

are input within 1.1 – 1.3 s, results 0.16 m maximum deflection of solar panel tip, i.e. node 27, during the maneuver process as shown in Fig. 6. This deflection is only 11% of the steady-state vibration amplitude after maneuver under the bang-bang torque inputs. Compared with solar panel's length of 12 m, this deflection is about 1.3%. In this case, the fuelling duration for roll is 4.888 s, while the fuelling duration for yaw is 4.684 s. Compared to the 21.528-s and 16.444-s lengths of roll and yaw fuelling durations of bang-bang inputs, respectively, these inputs consume fuel of 25.2% only. The attitude maneuver duration in this case is about 4.5 times of the bang-bang one.

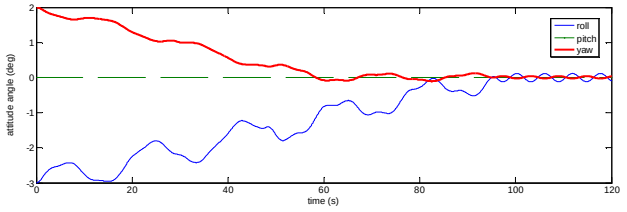

(a)

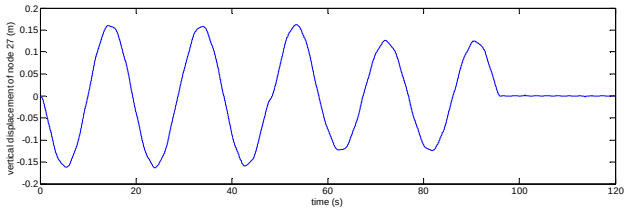

(b)

Figure 6: Time responses of Case 1: (a) attitude angle of the main body, and (b) local vertical displacement of node 27.

The application of 1.9 – 2.8 s lengths, or about twice of Case 1, of pulses duration in the torque inputs will result larger maximum deflection of node 27 during the transient response. We can see in Case 2 that the maximum deflection of the node 27 becomes 0.28 m at about t = 6 s as shown in Fig. 7. This deflection is about 2.3% of the solar panel's length. In this case, the fuelling duration for roll is 8.028 s, while the fuelling duration for yaw is 11.124 s. The total length of fuelling durations of roll and yaw inputs is 50.4%, while the maneuver duration is about 1.6 times of the bang-bang ones.

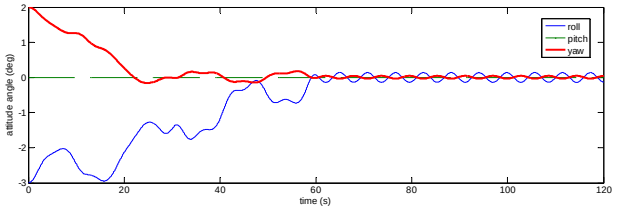

(a)

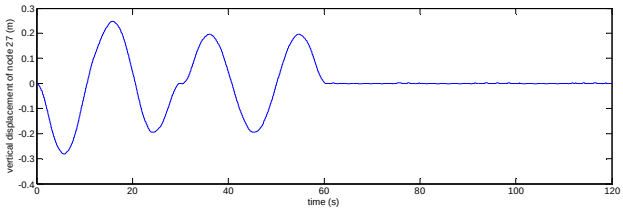

(b)

Figure 7: Time responses of Case 2; (a) attitude angle of the main body, and (b) local vertical displacement of node 27.

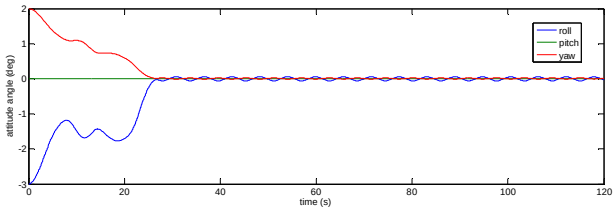

(a)

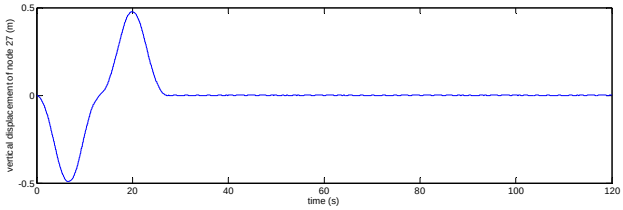

(b)

Figure 8: Time responses of Case 3: (a) attitude angle of the main body, and (b) local vertical displacement of node 27.

When the 2.7 – 4.3 s lengths of pulses duration, or about three times of those used in Case 1, are applied, the maximum deflection of node 27 during the transient response becomes larger than the resulted one in Case 2. We can see in Fig. 8 that the maximum deflection of the node 27 becomes 0.49 m, which happens at about t = 7 s. This deflection is about 4.1% of the solar panel's length. The fuelling durations for roll and yaw are 17.008 s and 11.124 s, respectively. The maneuver duration is about 1.3 times, while the total length of roll and yaw fuelling durations is 74.1% of the bang-bang ones.

6.0 CONCLUSION

Attitude maneuver of the flexible satellite induces the vibration of flexible members as well as the main body oscillation. Using the bang-bang input, the flexible satellite has poor attitude accuracy after slew maneuver. For desired angle displacements of 3° in roll and 2° in yaw only, the satellite studied in this paper has 3.7° and 1.3° residual roll and yaw angle oscillations, respectively, and results 1.46-m amplitude of steady-state vibration of the tip of 12-m solar panel's length.

Shaped inputs show their capability to reduce steady-state oscillation and vibration after the maneuvers slightly. For the shaped inputs, eight impulses in fuel-efficient types are utilized here with the fourth and fifth impulses are at the same location.

For the maneuver duration less than 100 s simulated in the paper using about similar duration length of fuelling pulses, the maximum amplitudes of solar panel's tip deflection become smaller than 0.5 m. The longer the fuelling duration lengths in the inputs, the larger the maximum deflection of the tip during maneuver's transient response will be.

ACKNOWLEDGEMENT

The author would like to convey a great appreciation to Universiti Teknologi PETRONAS for supporting this research.

REFERENCE

1. Singhose, W., Bohlke, K. and Seering, W.P. (1995). *Fuel-efficient shaped command profiles for flexible satellite*, AIAA Guidance, Navigator, and Control Conference.
2. Parman, S. and Koguchi, H. (1998). *Rest-to-rest attitude maneuvers of a satellite with flexible solar panels by using input shapers*, Computer Assisted Mechanics and Engineering Sciences, Vol. 5 (4), pp: 421-441.
3. Parman, S. and Koguchi, H. (2000). *Fuel-efficient attitude maneuvers of flexible satellite with residual vibration reduction into an expected level*, Computer Assisted Mechanics and Engineering Sciences, Vol. 7 (1), pp: 11-21.
4. Parman, S. and Koguchi, H. (1999). *Controlling the attitude maneuvers of flexible satellite by using time-optimal/fuel-efficient shaped inputs*, Journal of Sound and Vibration, Vol. 221 (4), pp: 545-565.
5. Parman, S. and Koguchi, H. (1999). *Rest-to-Rest Attitude Maneuvers and Residual Vibration Reduction of a Finite Element Model of Flexible Satellite by Using Input Shaper*, Shock and Vibration, Vol. 6 (1), pp: 11-27.
6. Parman, S. (2013). *Controlling attitude maneuvers of flexible satellite based on nonlinear model using combined feedback-feedforward constant-amplitude inputs*, 10th IEEE International Conference on Control and Automation (ICCA).
7. Robertson, M.J. and Singhose, W.E. (2005). *Closed-Form Deflection-Limiting Commands*, American Control Conf., June 8-10 (Portland, OR, USA), Paper ThA11.3.
8. Robertson, M.J. (2008). *Transient Deflection Performance Measures for Command Shapers*, American Control Conf., June 11-13 (Seattle, Washington, USA), paper ThC10.1.
9. Bogner, F.K., Mallet, R.H., Minick, M.D. and Schmidt, L.A. (1965). *Development and evaluation of energy searh methods of nonlinear structural analysis*, Flight Dynamics Lab. Report, AFFDL TR 65-113.

Journal of Ocean, Mechanical and Aerospace
-Science and Engineering-, Vol.24

October 30, 2015

Wave Climate Variations in Indonesia Based on ERA-Interim Reanalysis Data from 1980 to 2014

Muhammad Zikra,[a,*] and Putika Ashfar[b]

[a)] *Department of Ocean Engineering, Institut Teknologi Sepuluh Nopember (ITS), Surabaya, Indonesia*
[b)] *Coastal Environmental Laboratory, Department of Ocean Engineering, Institut Teknologi Sepuluh Nopember, Indonesia*

*Corresponding author: mzikro@oe.its.ac.id

Paper History

Received: 16 October 2015
Received in revised form: 27 October 2015
Accepted: 29-October-2015

ABSTRACT

In this study, temporal variation in significant wave height are studied using ERA-Interim reanalysis data from ECMWF (European Centre for Medium-Range Weather Forecasts) for 35 years period from 1980-2014. The ERA-Interim reanalysis data provides wind speed and wave height data with resolution of 1 x 1 degree. This paper studied monthly variation in significant wave height and wind speed by creating monthly data and taking the mean of those months over a period 35 years. The results show that the mean wind speed and significant wave height in the South of Java Sea have an increasing trend for all month.

KEY WORDS: *Wave, wind speed, ERA-Interim*

1.0 INTRODUCTION

Indonesia as an archipelago country, especially in coastal area, is very vulnerable to climate change such as sea level rise, warmer ocean temperature and increased of wave height [1]. Numerous studies reported that climate change has a significant impact on the future of wind and wave climate condition [2][3][4].

Knowledge of wave climate change due to global warming is required for engineering purpose. Especially, knowledge about wave information in a certain area is important for all activities related to the marine sector. For example offshore industry, ship design for safety and seakeeping, marine transportation management, renewable wave energy etc. Therefore, understanding the long-term variations in the wave parameter is key element for sustainable management of both offshore and coastal activities.

The objective of this study is to analyze the monthly variability of the wind and wave climate at Indonesia Sea based on the wind speed and significant wave height (SWH) obtained from ECMWF reanalysis ERA-Interim data for 35 years (1980 - 2014). ERA-Interim data has proved a better spatial resolution than ERA 40 to analysis SWH at North Sea [5]. This analysis study can serve as basis data source for possible wave energy evaluation projects in Indonesia.

2.0 DATA

In Indonesia, long-term wave records based on in situ measurements are still limited. Due to that reason, in this study, temporal variation in wind speed and significant wave height are studied using hindcasting model from ERA-Interim reanalysis data from ECMWF (European Centre for Medium-Range Weather Forecasts) for 35 years period from 1980-2014.

The ERA-Interim reanalysis data provides wind speed and significant wave height data with resolution of 1^o x 1^o. ERA-Interim is the first re-analysis using adaptive and fully automated bias corrections of satellite radiance observations [5] and contains improvements to ERA-40 such as the complete use of four-dimensional variation data assimilation from various kinds of sources such as scatterometers, altimeters, US wind profiler data, etc. For this study, 10 observation locations were chosen on the nearest of Indonesia sea. Those observation points are shown in the Figure 1 and names of each location is presented in Table 1.

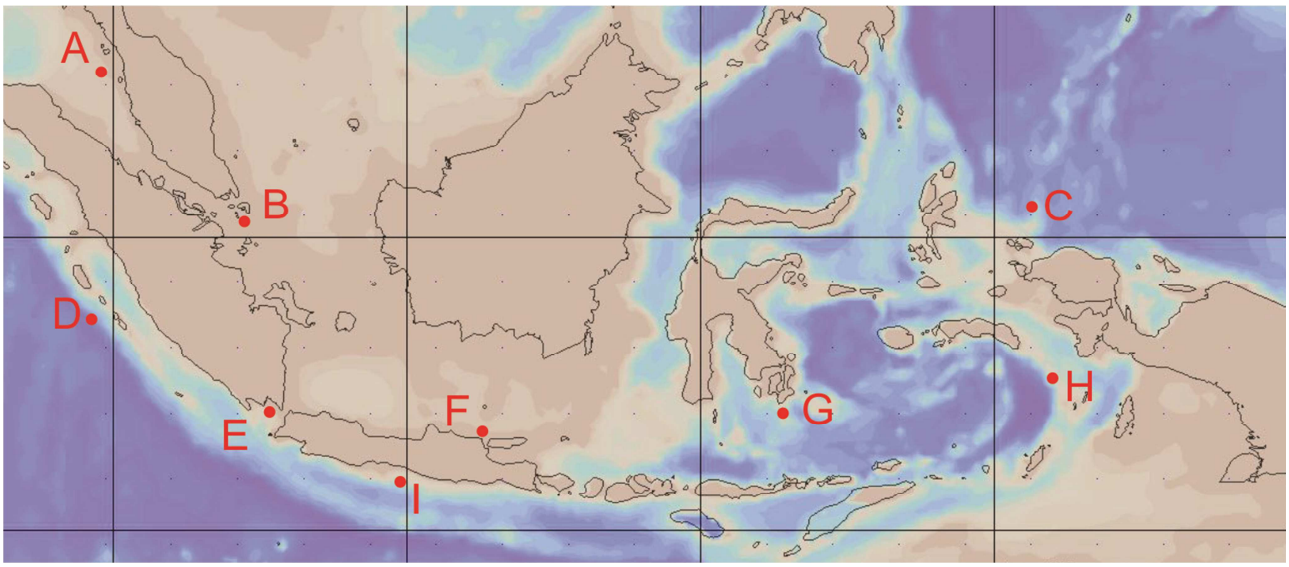

Figure 1: Observations points in Indonesia seas

Table 1: Observation points

Point	Coordinate	Location
A	3.75^0 N and 99.75^0 E	Malacca Strait
B	0.75^0 N and 105^0 E	Natuna sea, Riau Island
C	0.75^0 N and 130.50^0 E	Pacific Ocean
D	3.75^0 S and 99.75^0 E	Indian Ocean, Mentawai Island
E	6.00^0 S and 105.75^0 E	Sunda Strait
F	6.75^0 S and 112.50^0 E	Java Sea
G	6.75^0 S and 121.50^0 E	Flores Sea
H	2.25^0 S and 131.25^0 E	Banda Sea
I	110.5^0 S and 2.25 E	South of Java Sea

In this study, wind speed and significant wave heights (SWH) downloaded for the period 35 years from 1984 to 2014 at 6-hourly intervals. We studied variation in parameters wind speed and SWH by creating monthly data from the 6-hourly data and taking the mean of those months over a period of 35 years. Simple linear regression is used to estimate the linear trend (slope) of wind speed and wave height time series data:

$$y_t = a + bt$$

where t is specified number of time periods from t=0, y_t is forecast for time period t, a is the value of y at t and b is the slope of the line. The trend is the rate at which wind speed or wave height changes over 35 years period

3.0 RESULTS

The monthly mean wind speed trends are calculated for 35 years are shown in Table 2. Monthly mean wind speed trend at Natuna Sea, Pacific Ocean, Flores Sea and Banda Sea show negative trend from January to March. Other locations (Malacca strait, Indian Ocean and South of Java Sea) show an upward trend during January to March with maximum trend 3.18 cm.s-1/years.

The increasing trends have occurred in all month during a year for monthly mean wind speed in Malacca strait, Mentawai Island and South of Java Sea. South of Java Sea has a higher increasing trend of monthly mean wind speed with 4.2 cm.s-1/years. Meanwhile, the trend of monthly mean wind speed in Natuna Sea and Sunda strait has decreasing trends for all month with the value between -0.09 cm.s-1/years to -3.42 cm.s-1/years. Sunda strait has a higher decreasing trend on May with -3.42 cm.s-1/years. For other locations, the trends of monthly mean wind speed are varying depending on month during west monsoon or east monsoon seasons.

The monthly mean of significant wave height (SWH) trends are calculated for 35 years are shown in Table 3. For the trend of monthly mean SWH, Pacific Ocean, Banda Sea and South of Java Sea have increasing trend during all month. South Java Sea has the highest trend of mean significant wave height (SWH) with 5.05 cm/years on January as shown in Table 3.

Meanwhile, for other location, the trends of monthly mean SWH are varying depend on month. During March and April, all trend of monthly mean of significant wave height show increasing trend. Start from April, monthly mean SWH trend in Malacca strait show decreasing value become -0.84 cm/years. Same situation in Java Sea, start from May the trend of SWH become negative value until -4.08 cm/year on December.

Added, the present study shows the monthly mean of wind speed and significant wave height have a decreasing trend all month during 35 years period that in South of Java Sea, as shown in Figure 2 and 3, respectively.

Table 2: Trend of monthly mean wind speed during 1980- 2014

Month	Monthly Mean Wind Speed Trend (cm.s^{-1}/years)								
	A	B	C	D	E	F	G	H	I
January	2.23	-1.01	-0.41	0.46	-0.09	-1.87	-2.73	-0.41	0.37
February	1.73	-0.61	-2.47	1.11	-0.21	0.84	-2.86	-2.47	1.30
March	1.16	-0.26	-2.21	1.86	0.68	1.82	-0.81	-2.21	3.18
April	0.52	-0.29	0.46	-0.03	-2.04	1.23	1.62	0.46	1.26
May	0.80	-0.61	-0.11	0.19	-3.42	-0.08	2.36	-0.11	2.33
June	0.54	-1.46	-0.40	0.89	-2.97	-1.48	0.52	-0.40	2.93
July	1.43	-1.56	-0.20	0.96	-3.05	-2.47	0.10	-0.20	2.39
August	0.89	-2.34	-2.19	1.07	-2.51	-2.62	-2.81	-2.19	3.33
September	1.20	-0.99	-0.69	1.34	-1.36	-1.50	-2.59	-0.69	4.21
October	0.81	-0.42	0.79	0.28	0.42	-0.73	-1.61	0.79	2.75
November	0.05	-1.24	0.80	0.48	-1.19	-2.34	-2.38	0.80	0.37
December	1.10	-0.31	-2.91	0.63	-1.02	-4.08	-2.86	-2.91	0.57

Table 3: Trend of monthly mean significant wave height (SWH) during 1980- 2014

Month	Monthly Mean SWH Trend (cm/years)								
	A	B	C	D	E	F	G	H	I
January	0.20	0.04	0.76	-0.52	0.55	-1.87	-0.50	0.76	5.05
February	0.20	0.20	0.34	0.56	0.34	0.84	-0.47	0.34	2.09
March	0.20	0.55	0.38	0.37	0.61	1.82	0.02	0.38	2.70
April	-0.18	0.18	0.61	0.05	0.20	1.23	0.57	0.61	2.80
May	-0.19	0.22	0.51	-0.17	-0.11	-0.08	0.87	0.51	2.63
June	-0.37	0.09	0.56	-0.35	-0.19	-1.48	0.81	0.56	2.47
July	-0.29	0.03	0.60	0.03	-0.02	-2.47	1.11	0.60	2.73
August	-0.27	-0.03	0.10	0.16	0.04	-2.62	0.50	0.10	2.54
September	-0.20	0.17	0.19	0.14	0.52	-1.50	-0.02	0.19	0.17
October	-0.84	-0.40	0.51	0.17	0.59	-0.73	-0.30	0.51	2.29
November	0.07	-0.02	0.51	-0.07	0.29	-2.34	-0.04	0.51	5.05
December	-0.45	-0.20	0.14	0.01	0.30	-4.08	-0.20	0.14	1.85

4.0 CONCLUSION

Temporal variation of significant wave height in Indonesia sea are studied using ERA-Interim reanalysis data from ECMWF for 35 years period from 1980-2014. The ERA-Interim reanalysis data provides wind speed and wave height data with resolution of 1 x 1 degree. This paper studied monthly variation in significant wave height and wind speed by creating monthly data and taking the mean of those months over a period 35 years. The results show that the mean wind speed and significant wave height in the South of Java Sea have an increasing trend for all months.

ACKNOWLEDGEMENTS

The authors would like to thank DIKTI for providing research program under Grand Number 003246.167/IT2.11/PN.08/2015.

REFERENCE

1. Muhammad Zikra, Suntoyo, Lukijanto. 2015. Climate change impacts on Indonesian coastal areas. *Proceeding Earth and Planetary Science*. 14. DOI: 10.1016/j.proeps.2015.07.085

2. IPCC. 2007. *Contribution of Working Group I to the Fourth Assessment Report of the Intergovernmental Panel on Climate Change*. Cambridge, United Kingdom and New York, NY, USA: Cambridge University Press.
3. Muhammad Zikra, Hashimoto. N., Mitsuyasu. K., Sambodho K. 2015. *Monthly Variations of Global Wave Climate due to Global Warming*. Jurnal Teknologi. Vol. 74. No. 5. DOI: http://dx.doi.org/10.11113/jt.v74.4637.
4. Mori, N., Yasuda, T., Mase, H., Tom, T., & Oku, Y. 2010. Projection of Extreme Wave Climate Change under Global Warming. *Hydrological Research Letters*. 4: 15-19.
5. Dee, D.P., Uppala. Simmons. 2011. *The ERA-Interim Re-Analysis: Configuration and Performance of The Data Assimilation System*. Quarterly Journal of the Royal Meteorological Society. 137: 553-597
6. Tolman, Hendrik. L. 2014. User Manual and System Documentation of WAVEWATCH III version 4.18. *Environmental Modeling Center Marine Modeling and Analysis Branch*.

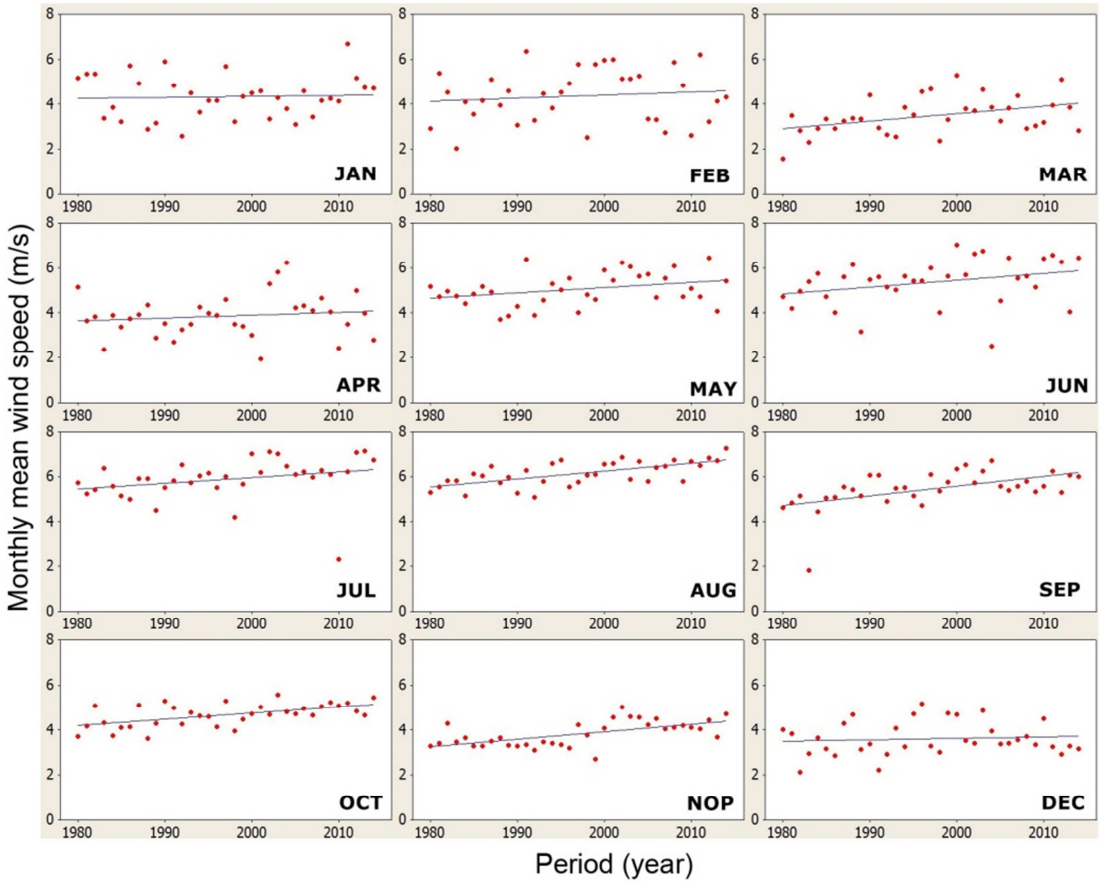

Figure 2: Variation of monthly mean wind speed in the South of Java Sea (Point I)

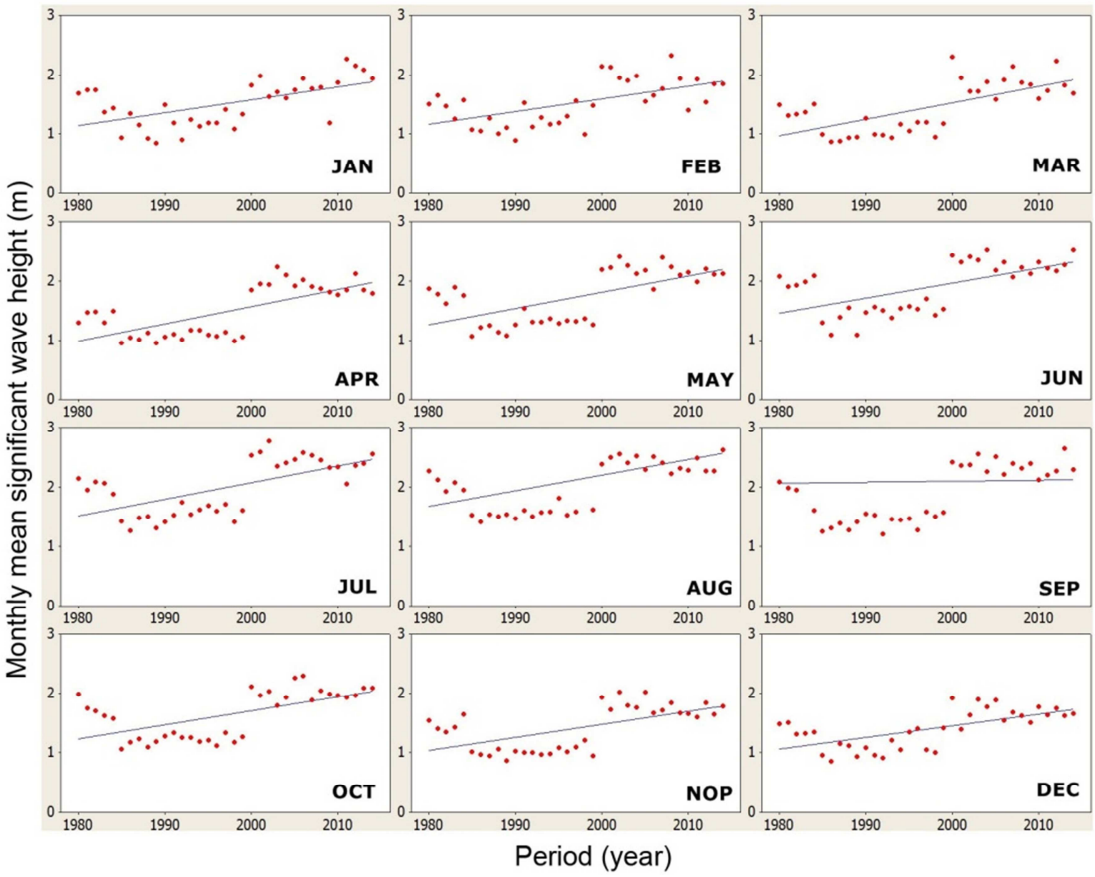

Figure 3: Variation of monthly means SWH in the South of Java Sea (Point I)

Publishing

ISOMAse
Resty Menara Hotel
Jalan Sisingamangaraja No.89
Pekanbaru-Riau, INDONESIA
http://www.isomase.org/

Editing

Building P-23, Room: 314
Department of Aeronautics,
Automotive & Ocean Engineering,
Faculty of Mechanical, Universiti
Teknologi Malaysia, MALAYSIA
http://web1.fkm.utm.my/

ISSN: 2354-7065

Publication

Teknik Mesin
Fakultas Teknik,
Universitas Riau, INDONESIA
http://www.unri.ac.id/en

Organizing

Ocean & Aerospace Research
Institute, Indonesia
Pekanbaru-Riau, INDONESIA
http://isomase.org/OCARI.php/

Supporting

Mechanical Chapter of the
Institution of Engineers,
INDONESIA

Malaysian Joint Branch Royal
Institution of Naval Architects &
Institute of Marine Engineering,
Science and Technology
-Southern Chapter (MJB RINA
&IMarEST – SC)-